




Mobilization of subcutaneous fascia contributes to the vascularization and function of acellular adipose matrix via formation of vascular matrix complex

Han Yang^a, Yidan Xu^a, Sousan Cheong^a, Cuiying Xie^b, Yufan Zhu^a, Shujie Xu^a, Feng Lu^{a,**}, Yunfan He^{a,*} 

^a The Department of Plastic and Cosmetic Surgery, Nanfang Hospital, Southern Medical University, 1838 Guangzhou North Road, Guangzhou, 510515, Guangdong, China

^b Clinical Pharmacy Center, Nanfang Hospital, Southern Medical University, 1838 Guangzhou North Road, Guangzhou, 510515, Guangdong, China

ARTICLE INFO

Keywords:

Fascia
Vascularization
Adipogenesis
Acellular extracellular matrix

ABSTRACT

Regenerative biomaterials are commonly used for soft-tissue repair in both pre-clinical and clinical settings, but their effectiveness is often limited by poor regenerative outcomes and volume loss. Efficient vascularization is crucial for the long-term survival and function of these biomaterials in vivo. Despite numerous pro-vascularization strategies developed over the past decades, the fundamental mechanisms of vascularization in regenerative biomaterials remain largely unexplored. In this study, we employed matrix-tracing, vessel-tracing, cell-tracing, and matrix analysis techniques, etc. to investigate the vascularization process of acellular adipose matrix (AAM) implants in a murine model. Here, we show that the mobilization of subcutaneous fascia contributes to the vascularization in AAM implants. Tracing techniques revealed that the subcutaneous fascia migrates to encase the AAM implants, bringing along fascia-embedded blood vessels, thus forming a vascular matrix complex (VMC) on the implant surface. Restricting fascia mobilization or removing fascia tissue significantly reduced AAM vascularization and hindered the regenerative process, leading to implant collapse at a later stage. Notably, VMC exhibited a dynamic matrix remodeling process closely aligned with implant vascularization. Our findings highlight the crucial role of subcutaneous fascia mobility in facilitating the vascularization of AAM implants, offering a novel direction and target for guaranteeing long-term survival and function of regenerative biomaterials in vivo.

1. Introduction

Repairing severe injuries or large soft tissue defects remains a major challenge in clinical practice worldwide. In recent decades, tissue engineering has offered promising alternative approaches to restore damaged tissues and organs using regenerative biomaterials [1]. A crucial aspect of the functional integration and long-term survival of these biomaterials in vivo is effective vascularization. However, the vascularization of regenerative biomaterials has not been thoroughly investigated [2,3]. Most studies have focused their effort on the researches of pro-vascular factors or biomaterials structure itself, while this study provide a novel perspective for the study of biomaterials vascularization, that is subcutaneous fascia.

Materials implantation is generally accepted to initiate vascularization from host vasculature by stimulating invasive microvessels into the implants [4]. However, the process by which the host vasculature connects with implants is not well understood. Most current knowledge suggests that implants cause tissue injury and trigger an inflammatory immune response known as the host foreign body reaction (FBR) [5,6]. FBR is characterized by the formation of a dense and avascular fibrous capsule around the implants at the terminal state, which can weaken the vascularization and integration of implanted materials with the host environment [7–9]. Recent studies, however, indicate that regenerative biomaterials, especially those derived from natural sources, may not provoke the typical FBR. Instead, these biomaterials generally elicit a mild, constructive immune reaction that promotes vascularization,

* Corresponding author.

** Corresponding author.

E-mail addresses: doctorlufeng@hotmail.com (F. Lu), doctorheyunfan@hotmail.com (Y. He).

<https://doi.org/10.1016/j.mtbio.2025.101461>

Received 29 August 2024; Received in revised form 11 December 2024; Accepted 3 January 2025

Available online 4 January 2025

2590-0064/© 2025 The Authors. Published by Elsevier Ltd. This is an open access article under the CC BY-NC-ND license (<http://creativecommons.org/licenses/by-nc-nd/4.0/>).

integration, and tissue regeneration [10]. Understanding how regenerative biomaterials govern vascularization will enhance biomaterial design, fostering the development of functional and long-lasting engineered structures.

Acellular extracellular matrix isolated from tissues and organs has emerged as promising regenerative biomaterials due to its spontaneous regeneration properties. Our previous studies demonstrated that the vascularization of acellular adipose matrix (AAM) rely on invasive microvessels from host vasculature at the implantation site [11–13]. Notably, this host vasculature system is located in a loose areolar connective matrix called subcutaneous fascia, which surrounds AAM implants [14]. In this study, we refer to the fascia matrix containing vasculature on the surface of AAM implants as the vascular matrix complex (VMC). Fascia is an uninterrupted viscoelastic membranous sheet that extends between tissues and organs throughout the body [15]. Subcutaneous fascia, also known as superficial fascia, plays a critical role in maintaining skin integrity and sustaining subcutaneous structures, including fatty tissue, blood vessels, nerves etc. [16]. Particularly, subcutaneous fascia also provides a structural scaffold for vessels and connects vessel walls by attaching to their adventitia [15]. Given its anatomical features and interactions with the vessels system, we hypothesized that fascia, along with its derived vasculature system, induces the vascularization of regenerative biomaterials *in vivo*.

In the current work, we explored the fundamental mechanisms of the vascularization process in regenerative biomaterials using an AAM transplantation model in mice. Utilizing matrix-tracing techniques, whole-mount staining, histopathology, streamgraph and correlation analysis, we identified that subcutaneous fascia and its embedded blood vessels migrated to form a VMC on the surface of AAM implants at the early stage. At late stage, invasive microvessels from the VMC infiltrate AAM implants, leading to implants vascularization and adipogenesis. In addition, we found that the VMC undergoes dynamic matrix remodeling, closely linked to the vascularization of both the VMC and the implants vascularization.

2. Methods

2.1. Animal models

Male C57BL/6J mice (6–8 weeks old) were provided by the Southern Medical University Laboratory Animal Centre and housed in micro-isolator cages at the Animal Experimental Center of Nanfang Hospital. All animal procedures adhered to the ethical guidelines of the National Health and Medical Research Council (China) and were approved by the Animal Ethics Committee of Nanfang Hospital.

2.2. Preparation of AAM

AAM was prepared using a method established in our laboratory [11, 13, 17]. With informed consent, human adipose tissue was collected from female patients undergoing abdominal liposuction. In brief, the obtained lipoaspirate was washed with sterilized saline, repeatedly centrifuged at 3000 g for 3 min to remove residual oils and blood, and then subjected to freeze-thaw cycles (−80 °C for 12 h, then thawed at 37 °C) for 3 times. It was then homogenized at 30,000 rpm for 1 min. The lipoaspirate sample was collected after centrifugation at 3000g for 3 min and subjected to a 6-h polar solvent extraction in 99.9 % isopropanol to remove remaining lipids. After 3 rinses with PBS, the sample was mixed with 0.1 % aqueous sodium deoxycholate and agitated for 12 h for decellularization. Finally, the sample was sterilized with 0.1 % peracetic acid in 4 % ethanol for 4 h and stored at −80 °C until use.

2.3. Xenotransplantation models

AAM was sheared under aseptic conditions and injected into the mice using an 18-gauge needle. The C57BL/6J mice were anesthetized with

an intraperitoneal injection of 50 mg/kg pentobarbital sodium (Sigma, USA), and 0.25ml/side AAM was subcutaneously injected into the bilateral dorsal regions. The animals were sacrificed at 3, 7, 14, 28 and 90 days post-implantation (dpi). The grafts and overlying murine skin were harvested for analysis.

2.4. *In situ* matrix tracing of subcutaneous fascia

Labeling of subcutaneous fascia matrix was performed as described by Correa-Gallegos et al. [18]. Briefly, 1 mM Alexa Fluor 647 NHS ester (AF647 NHS) (A20006, Thermo Fisher Scientific, Waltham, MA) in physiological saline was prepared and 200 μ l labeling buffer was subcutaneously injected per side one day before AAM implantation. AAM samples were collected at 7, 14 and 28dpi for further analysis.

2.5. Labeling of fascia-derived vessels and cells in animals

One day before AAM implantation, C57BL/6J mice received 200 μ l injection of 1 mM DyLight 649 lycopersion esculentum lectin (649 TL) (L32472, Thermo Fisher Scientific) and 200 μ l lipophilic vybrant DiI dye (G1705, Servicebio), prepared at a 1:400 dilution into the subcutaneous fascia of each bilateral dorsal region using a 30-gauge needle to label vessels and cells, respectively. Mice were sacrificed, and VMC and AAM implants were harvested for histology and imaged by fluorescence microscopy according to schedule.

2.6. Implantation of ePTFE membrane and VMC-removal models

Due to its high biocompatibility, biostability, and non-adhesiveness, expanded polytetrafluoroethylene (ePTFE) membranes are widely used to increase implantable device tolerance and decrease postoperative incision adhesion in clinical settings [19,20]. ePTFE's was used to prevent integration and interaction with surrounding tissues and fluids [19]. Correa-Gallegos et al. used ePTFE to block subcutaneous fascia matrix migration toward wound sites [18]. Similarly, in this study, ePTFE membranes were used to block the migration of subcutaneous fascia towards AAM implants. Briefly, two 1 cm incisions were made on both side of the dorsal skin of mice, and the subfascial layer was exposed using blunt separation. Sterile 16 mm \times 8 mm ePTFE impermeable membranes (Dualmesh, GORE) were implanted between the back muscle and subcutaneous fascia on the left side. The wound was sutured, followed by the injection of AAM between the ePTFE membrane and back muscle. The right sham control underwent the same procedure without the implantation of the ePTFE membrane. At 14dpi, all AAM implants were collected for further analysis.

To further investigate the role of VMC in AAM vascularization, VMC removal was performed. In AAM implantation models, 1 cm incisions were created on both sides of dorsal skin to expose AAM implants by blunt separation. In the VMC-removal group, VMC on the implant surface were carefully removed, while VMC was separated from AAM graft by blunt dissection without removal in the sham surgery group (sham). The incisions of both groups were closed with 6-0 nylon sutures. The implants were harvested for analysis as schedule, and their volume was measured using the fluid displacement method.

2.7. Histopathology and immunofluorescent staining

Samples were fixed, embedded, and sectioned into 4–6 μ m slices. Sections were placed onto charged glass slides and baked at 65 °C for 45 min to dry. After dewaxing and rehydration, hematoxylin and eosin (H&E) staining (G1120, Solarbio), Sirius red staining (G1472, Solarbio), Masson trichrome staining (G1340, Solarbio) and immunohistochemistry (IHC) were performed according to the manufacturer's instructions. Sirius red staining was imaged under bright field and polarized light (NIKON Eclipse ci).

For immunofluorescent staining, paraffin sections were incubated

overnight at 4 °C with anti-CD31 (ab28364, Abcam, Cambridge, MA) and anti-Perilipin-1 antibodies (GP29, Progen, Germany). Sections were then incubated with secondary antibodies, counterstained with DAPI, and observed under a confocal microscope (LSM 980, Carl Zeiss). Only CD31-positive areas with clearly defined luminal structures were counted as blood vessels, while positive regions lacking lumens were excluded from the analysis.

2.8. Whole-mount staining and scanning electron microscopy (SEM) of VMC

VMC samples were fixed with 4 % paraformaldehyde and washed with PBS before whole-mount staining. Samples were permeabilized with 0.3 % Triton-X 100 in 1× PBS for 10 min and blocked in 10 % goat serum in PBS for 1 h. After overnight incubation with 649 TL, Bodipy 493/503 (HY-D1614, MCE, New Jersey, USA) and AF647 NHS at 4 °C, samples were rinsed and observed under a confocal microscope (LSM 980, Carl Zeiss).

For SEM analysis, VMC samples were fixed in an electron microscope fixative (G1102, Servicebio) at room temperature for 2 h and then transferred to 4 °C for preservation. After washing in PBS three times, samples were blocked at room temperature with 1 % OsO₄ for 2 h. After another three washes in PBS, samples were gradually dehydrated in ethanol and isoamyl acetate (SinaophazGroup Chemical Reagent Company, 10003128). Samples were then dried, attached to metallic stubs using carbon stickers, and sputter-coated with gold. Finally, samples were imaged with a scanning electron microscope (Hitachi, SU8100).

2.9. Quantification of collagen fiber architecture and types

Quantitative analysis of collagen fiber architecture of AAM implants and VMC samples was performed on images of Sirius red-stained tissue sections using the CurveAlign framework (<http://loci.wisc.edu/software/ctfire>) [21]. This framework includes two separate but linked packages, “CurveAlign” and “CT-FIRE”. CurveAlign analyzes fiber orientation and alignment by directly extracting individual fibers, while CT-FIRE quantifies fiber metrics, such as length, width, angle and straightness. The CT-FIRE could also extract other variables such as fiber density of region of interest and the spatial relationship between fibers and associated boundary. The average fiber parameters of each sample were used for statistic analysis.

Quantitative analysis of collagen fiber types in AAM implants and VMC samples was performed using Sirius red-stained sections with ImageJ software (NIH Image). Larger collagen fibers appear yellow or orange, while finer collagen fibers (including reticular fibers) appear green under polarization microscopy. Identification of collagen fiber types follows the hue definitions (red 2–9 and 230–256, orange 10–38, yellow 39–51, and green 52–128) developed by Zhang et al. [22]. Type I collagen (Col-I) exhibited red birefringence, type II collagen (Col-II) orange birefringence, type III collagen (Col-III) green birefringence, and type IV collagen (Col-IV) weak yellow birefringence [23]. The area fraction of red, orange, yellow, and green were calculated, and a histogram of the hue slice image was obtained and analyzed.

2.10. Principal component analysis (PCA) of VMC

PCA was performed on the quantification of collagen fiber architecture and types with the center positioned to mean zero and scaled to unit variance using the `prcomp` function in R (4.3.2). The plot was generated using `ggplot2` and `FactoMineR` packages with a 95 % confidence interval.

2.11. Correlation analysis between collagen fiber characteristics and vascularization

Spearman’s correlation analysis was used to investigate the

correlation between collagen fiber architecture and vascularization in AAM implants and VMC. Correlation plots were generated using `ggstatsplot` and `cowplot` with 95 % confidence intervals. `Streamgraph` was used to show the changes in parameters of fiber architecture, vascularization and adipogenesis, with plots generated using `ggstream` in R.

2.12. Statistical analysis

Data are presented as means ± SEM and analyzed using Prism 9.5 (GraphPad, La Jolla, CA). Student’s *t*-test (unpaired and two-tailed) was performed for two-group comparisons. Comparisons of more than two groups were performed with one- or two-way ANOVA. *P* values: * < 0.05, ** < 0.01, *** < 0.001, **** < 0.0001.

3. Results

3.1. Vascularization appears earlier in VMC than AAM implants

Fig. 1 showed the morphology and the formation process of VMC from 3 dpi to 90 dpi. Initial VMC formation is observed on the surface of AAM implants as early as 3 dpi, with visible vessels formation at the edge of AAM implants by 7 dpi (Fig. 1A). Histological analysis shows that vascularization peaks at 14 dpi in VMC, earlier than the 28 dpi peak in AAM implants (Fig. 1B, E). The vascular structures in VMC also demonstrate greater maturity, indicated by larger lumen diameters at 14 dpi compared to AAM implants (Fig. 1B).

3.2. Subcutaneous fascia-derived vasculature contributes to the formation of vasculature in VMC

VMC forms a vasculature-containing connective matrix on the surface of AAM implants. Morphological and pathological assessments reveal that the vasculature in VMC originates from the surrounding host vasculature system (Fig. 2A and B). At 28dpi, significant vascular sprouts from VMC (red vessels) into AAM implants can be observed (Fig. 2C). Vessel-tracing technique confirm that these VMC vessels are derived from the surrounding subcutaneous fascia, as shown by fluorescent labeling (Fig. 2D–G).

3.3. AAM implant elicited mild host reaction

The host reaction to AAM implants is milder compared to silicone implants. Evaluating extracellular matrix deposition on implant surfaces reveals a typical fibrous capsule around silicone implants, while AAM implants show a loose matrix deposit (Fig. 3A and B). Quantitative analysis reveals that the thickness, cell density (normalized by areal measurement) and collagen fiber density are significantly higher in the silicone group than in the AAM group. In addition, sites of fiber aggregation, indicative of capsular contracture, are absent in the AAM group, suggesting a milder host reaction in vivo. scRNA-seq analysis (data not shown) identified that predominant cell populations within VMCs are stromal cells, fibroblasts, vascular-associated immunomodulatory stromal cells (VA-iSCs), and macrophages, with stromal cells and fibroblasts comprising the major population and macrophages constituted a minor proportion of all cell populations in VMC. IHC results revealed that these macrophage cells are mainly pro-inflammatory phenotype (M1) at 3 dpi and anti-inflammatory (M2) phenotype from 7 dpi to 90 dpi (Fig. 3C and D). The absence of prolonged M1 macrophages or foreign body giant cells (FBGCs) [24,25]—hallmarks of a classic foreign body response—indicates that VMC formation is possibly driven by fascia-derived stromal cells rather than a classic foreign body reaction.

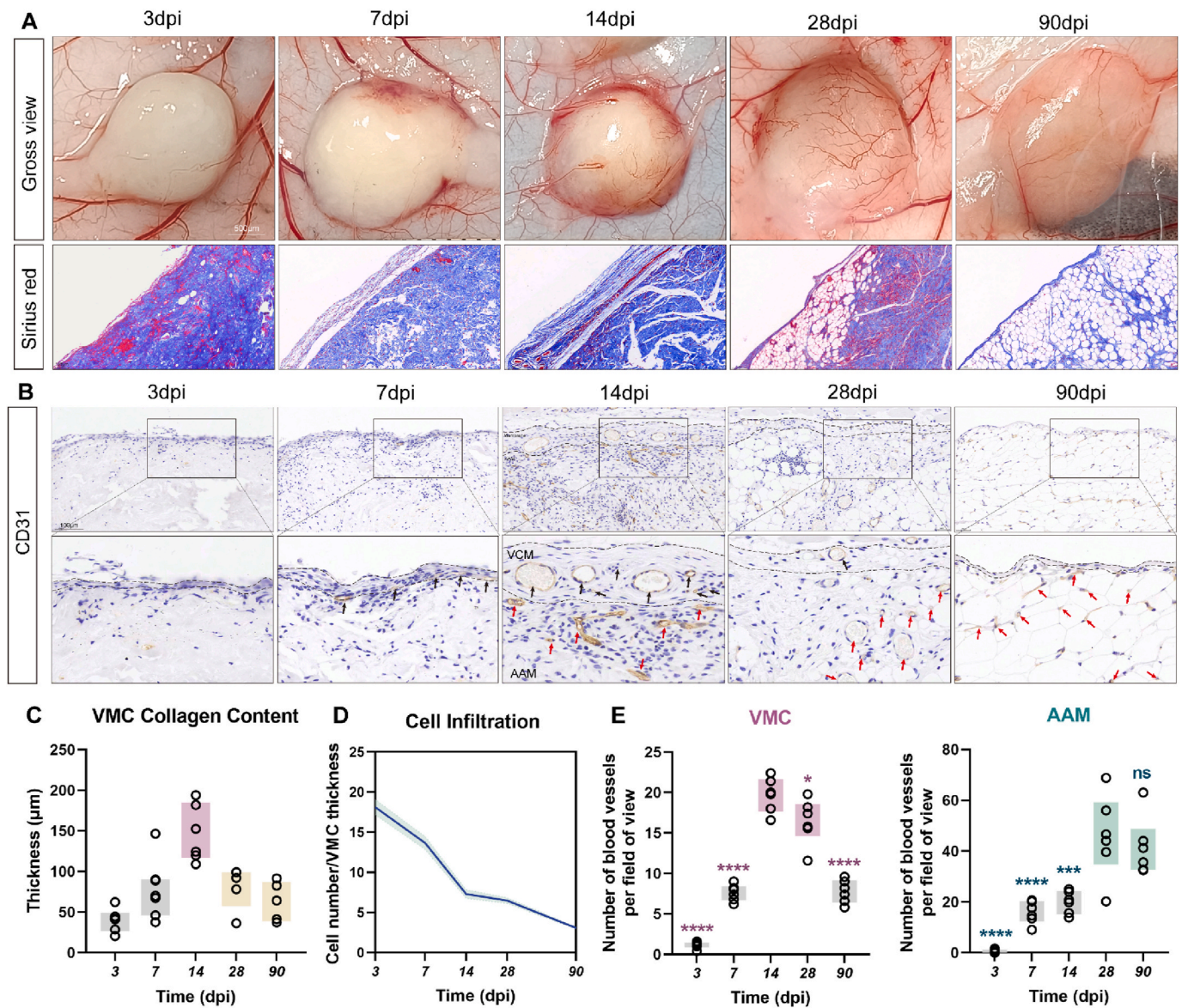


Fig. 1. Vascularization of VMC and AAM implants. (A, C and D) Morphological observation (top) and Masson trichrome staining (bottom) of AAM implants and VMC. Black dotted lines indicate the range of VMC. Individual values, $n = 5$ to 7 per group for VMC collagen content and 4 per group for cell infiltration, 95% confidence interval (CI). (B) CD31 staining for blood vessels (top) and higher magnification of the insets (bottom). Black dotted lines indicate the range of VMC. Black arrows indicate the blood vessels in VMC. Red arrows indicate the blood vessels in AAM. (E) The angiogenesis of VMC (left) and AAM (right) change over time. Comparing to “14 dpi” group, t -test, $n = 5$ to 6 per group (left); Comparing to “28 dpi” group, t -test, $n = 5$ to 6 per group (right). 95% CI.

3.4. Migration of subcutaneous fascia contributes to the majority of VMC formation

Although AAM implants do not elicit a typical FBR, the formation process of matrix scaffold on the implant surface still remains to be explored. In this study, we use matrix-tracing technique and cell-tracing technique to label surface matrix and fascia-derived cells beforehand. Tracing results demonstrate that subcutaneous fascia migrates to encase the surface of AAM implants as early as 7 dpi (Fig. 4A). Quantitative analysis reveals that fascia-derived matrix accounts for $82.52 \pm 2.07\%$, $83.38 \pm 2.97\%$ and $80.74 \pm 2.19\%$ of the total matrix scaffold in VMC at 7, 14, and 28 dpi respectively (Fig. 4D). To further investigate the contribution of subcutaneous fascia in VMC formation, we blocked fascia migration by implanting an inert medical ePTFE membrane between subcutaneous fascia and AAM implants (Fig. 5A). Quantification of collagen content shows that ePTFE membrane implantation significantly reduces VMC thickness by $73.92 \pm 2.31\%$ (mean \pm s.e.m.)

compared to controls (Fig. 5B). Together, our data indicate that subcutaneous fascia migration contributes to the majority of VMC formation in AAM implants.

Cell-tracing results demonstrate that fascia-derived cells migrated to VMC as early as 7 dpi (Fig. 4E and F). Quantitative analysis reveals that fascia-derived cells contribute to the cell population in VMC, accounting for $25.73 \pm 4.75\%$ at 7 dpi, and increasing to $60.61 \pm 3.92\%$ and $35.60 \pm 5.42\%$ at 14 and 28 dpi, respectively (Fig. 4F).

3.5. VMC contribute to the long-term survival and function of AAM implants

To investigate the influence of VMC on the fate of AAM implants, VMC was surgically removed at 7dpi and 14dpi respectively, stages when VMC forms (Fig. 5C and D). Morphological and histologic images show that implants in VMC-removal group exhibit atrophic appearance, necrotic cavities, and degenerative histologic characteristics compared

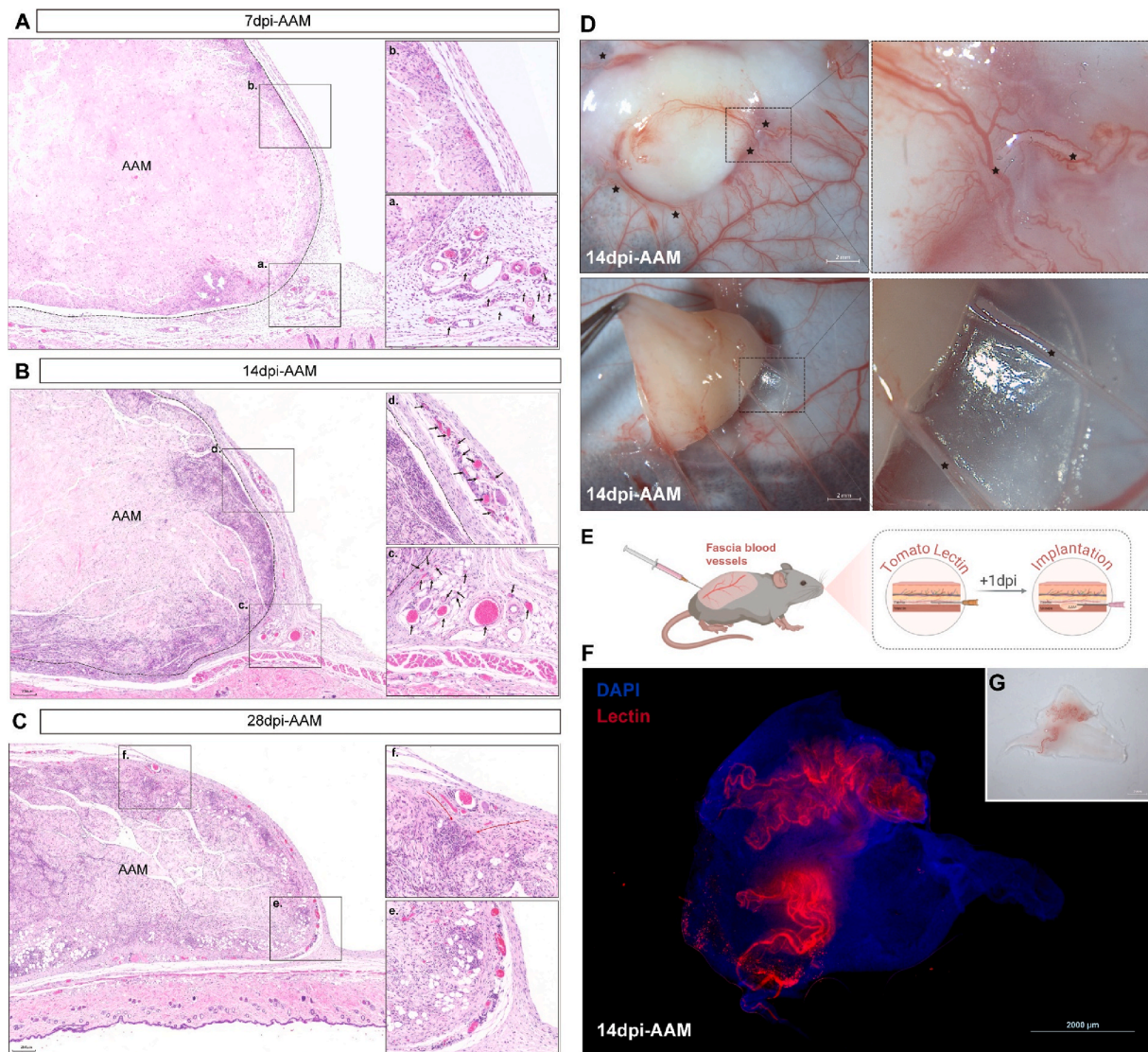


Fig. 2. Fascia is a major blood vessels source for implantation. (A, B and C) The localized and initial fascia blood vessels around implantable AAM at the first two weeks and the migrating and crossing fascia blood vessels at 28dpi. (D) Morphological images of AAM in vivo at 14dpi. Black stars indicate the blood vessels recruited from surrounding subcutaneous fascia. (E) Fascia blood vessels labeling with 649 TL one day before AAM implantation. (F) Whole-mount staining and (G) morphological image of the same explanted VMC at 14dpi.

to controls (Fig. 5D). Volume retention in VMC-removal groups significantly decreases at 28 and 90 dpi, with more pronounced effects observed in the 14 dpi-VMCR group (Fig. 5E). Similarly, VMC removal leads to reduced vasculature and adipogenesis in AAM implants, with worse outcomes in the 14 dpi-VMCR group (Fig. 5F–L). Collectively, these results indicate that VMC is critical for maintaining the volume retention and function of AAM implants.

3.6. Spontaneous angiogenesis and adipogenesis in VMC

The characteristic of VMC was investigated. Gross observation shows that VMC is a translucent, viscoelastic membranous containing a vasculature system (Fig. 6A). SEM and immunofluorescence staining show scattered adipocytes along vessels early by 14 dpi (Fig. 6A bottom, C). Whole-mount staining of VMC exhibits a vascularized adipose tissue within the matrix. Quantification analysis reveals that the vasculature area in VMC increases from 3 to 14 dpi and gradually decreases thereafter (Fig. 6C). Bodipy staining of VMC shows an increase in adipose tissue area from 7 to 28 dpi, reaching approximately $18.68 \pm 2.49\%$ by 28 dpi (Fig. 6C and E). Notably, AAM implants show delayed vasculature

compared to VMC, with vasculature peaking at 28 dpi (Fig. 6D, F left). Quantification of Perilipin-1 also reveals delayed adipogenesis in AAM, with significant adipogenesis detected only by 28 dpi, peaking at 90 dpi (Fig. 6F right).

3.7. Collagen fiber remodeling in VMC and AAM implants

Collagen type proportions in VMC change dynamically from 3 to 90 dpi (Fig. 8A). Quantification analysis demonstrates that Col-II, Col-III and Col-IV accounts for the major collagen components at all time points, with Col-II having the highest proportion, which decreases from 3 to 14 dpi and increases afterwards. Proportions of Col-III and Col-IV increase until 14dpi and then decrease (Fig. 8D). There is an increase in the Collagen III/I ratio from 3 to 14 dpi, which then decreases. Similarly, the expression of the basement membrane protein Fibronectin is dynamic, showing weaker expression in the early phase (3 dpi) and the late phase (90 dpi) but peaking during the intermediate phase (7–28 dpi) (Fig. 8B and C). This pattern highlights the temporal remodeling of VMC's extracellular matrix components during tissue regeneration.

The architecture of collagen fiber in VMC reveals that there also

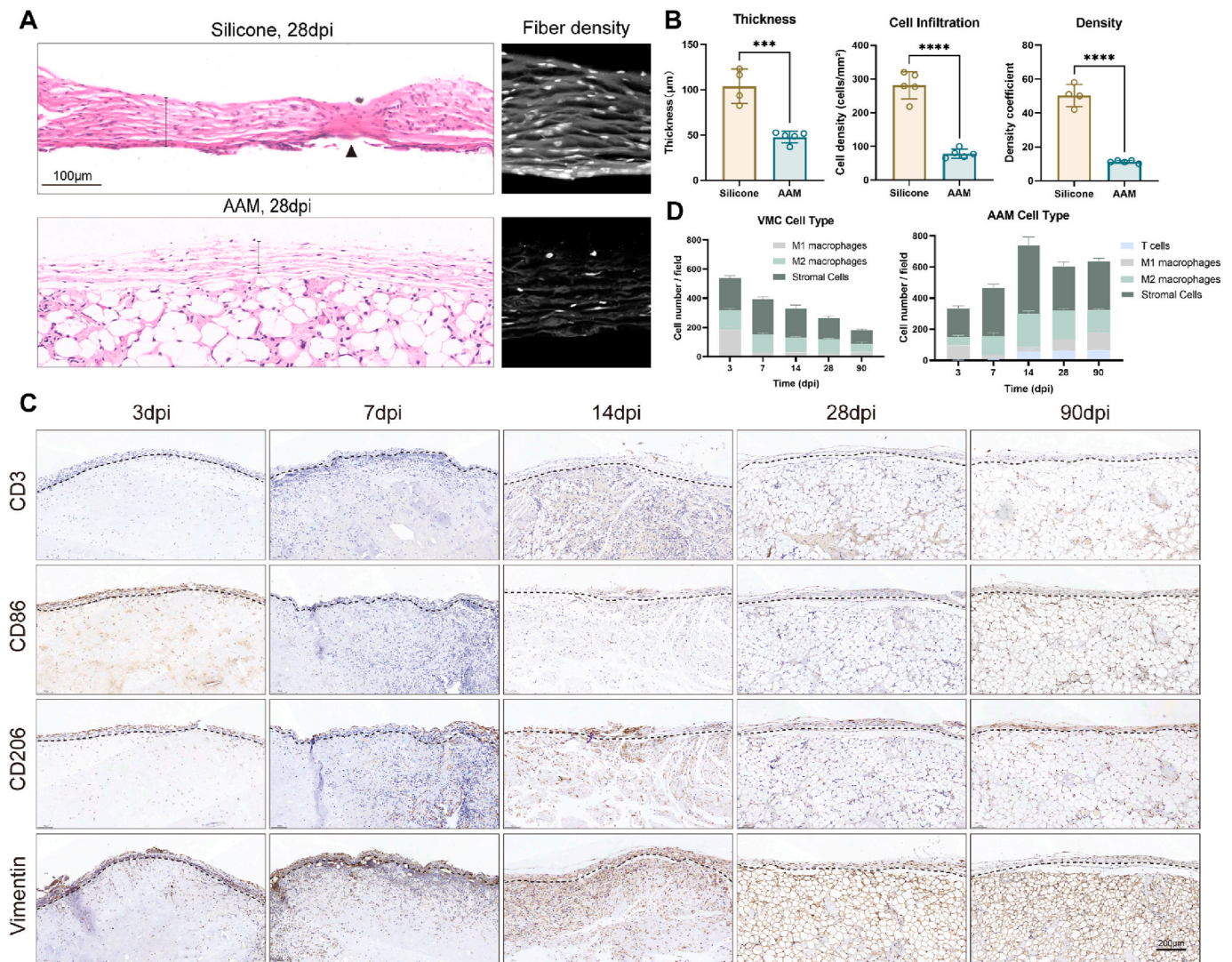


Fig. 3. AAM implant elicited mild host reaction. (A) H&E staining and (B) morphological analysis of implanted silicone and AAM at 28dpi. Black arrow indicates the contracture site on the silicone capsule. Black lines indicate the different thickness of the silicone capsule and VMC. T test, $n = 4$ to 5 (silicone) and 5 (AAM). 95 % CI. (C) CD3, CD86, CD206, Vimentin staining for T cells, M1 macrophages, M2 macrophages, and stromal cells. Black dotted lines indicate the range of VMC. (D) The cell numbers of M1 macrophages, M2 macrophages, stromal cells and T cells in VMC and AAM change over time. $N = 3$ per group. 95 % CI.

remains dynamic changes of fiber alignment, length, width, angle and density (Fig. 7A). Fiber alignment increases from 3 to 14 dpi and remains steady afterwards (Fig. 7Ba), while fiber density exhibits a slight decrease from 3 to 7 dpi, increases until 28dpi, and then decreases (Fig. 7Bd). Fiber length increases until 14 dpi and then decreases (Fig. 7Bb), and fiber width decreases until 28 dpi before increasing (Fig. 7Bc). Fig. 8E exhibits the images of collagen fibers in tissue interfaces between AAM and VMC sides at all time points (Fig. 8E). Quantification analysis in tissue interfaces reveals a significant higher fiber density in AAM than in VMC early on (3dpi to 14dpi), but similar densities by 28 and 90dpi (Fig. 8F). A notable negative correlation between density disparity and vessel number in AAM implants by correlation analysis suggests high collagen fiber density in AAM implants at early stage may hinder VMC-derived vessels invasion (Fig. 8G). A similar fiber density in tissue interfaces may partly explain the appearance of obvious ingrowth of vessels in AAM implants at 28 dpi.

3.8. Collagen fiber remodeling and vasculature development in VMC

The correlation analysis between collagen fiber remodeling and vasculature development in VMC was explored. According to PCA result,

the remodeling process of collagen fibers in VMC can be divided into three stages: early (3–7 dpi), middle (14 dpi) and late (28–90 dpi), as the collagen fiber characteristics and collagen types are highly similar in each stage (Fig. 8H). The PCA result differentiates VMC fibers into three distinct modes: dispersed thick and short collagen at early stage, dispersed thin and long collagen at middle stage, and aggregated blended thick and thin collagen at late stage. From early to middle stages, collagen transitions from disorganized thick and short fibers to organized thin and elongated fibers. Collagen fiber alignment, Col-III% and Col-IV% positively correlate with vasculature development in early to middle stages (Fig. 9Aa and 9Bb, h), while collagen fiber width and Col-II% show significant negative correlations (Fig. 9Ad and 9Bf) (see Fig. 10).

4. Discussion

Efficient vascularization is one of the key factors for the long-term survival and function of regenerative biomaterials in vivo. Traditional research on materials vascularization has primarily focused on the foreign body response to implants. However, recent studies, including our own, have come to realize that regenerative biomaterials tend to

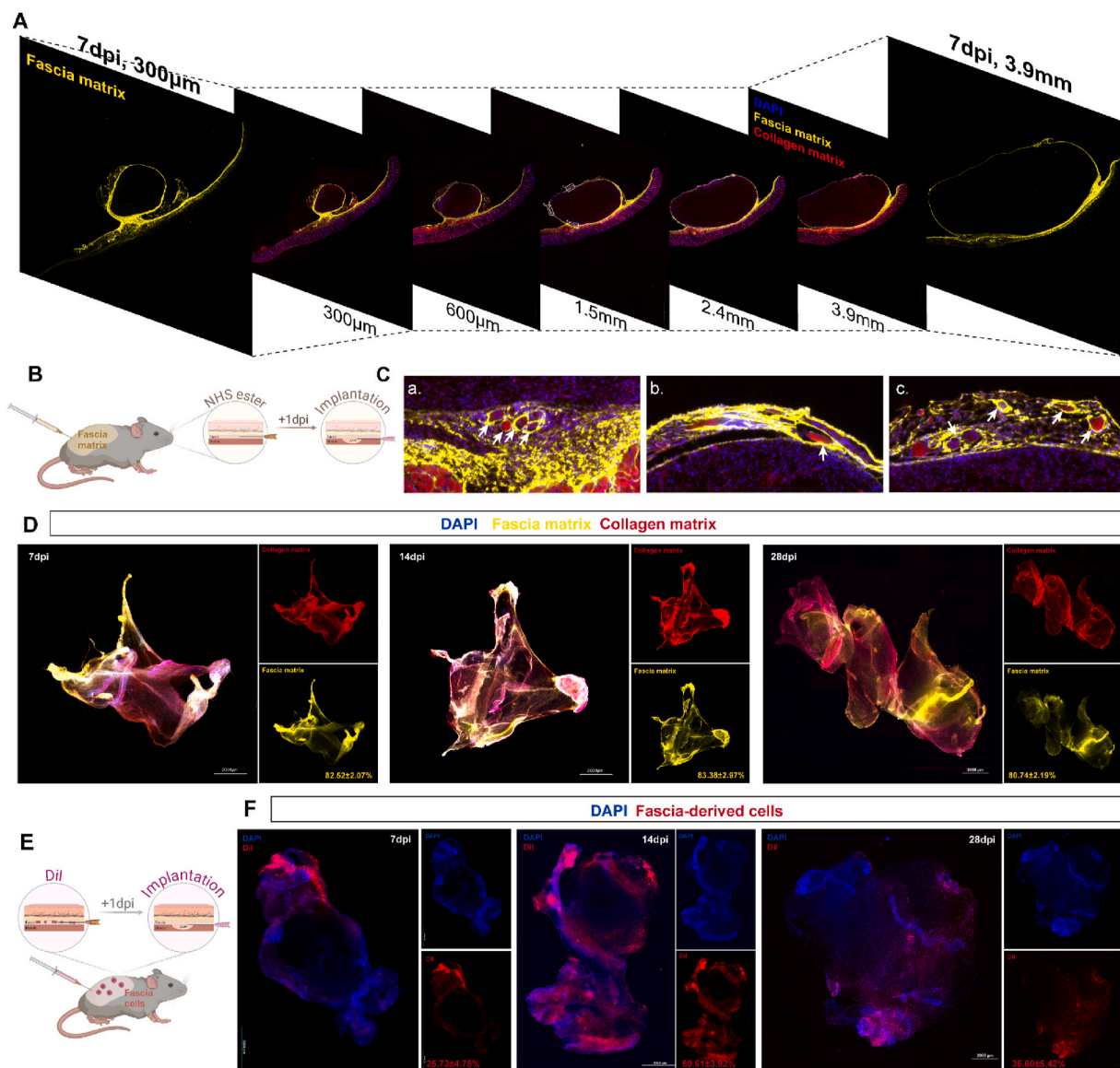


Fig. 4. VMC originated from fascia matrix instead of foreign body reaction. (A and C) Matrix-traced grafts at 7dpi and VMC blood vessels wrapped by fascia-derived matrix (a–c). White arrows indicate the blood vessels surrounded by fascia-derived matrix. (B) Matrix tracing of fascia in situ by AF647 NHS ester labeling one day before AAM implantation. (D) Whole-mount staining of fascia matrix labeling VMC at 7, 14 and 28dpi. Data are mean \pm s.e.m.; $n = 5$ (7dpi), 8 (14dpi) and 5 (28dpi). (E) Fascia cells labeling with DiI one day before AAM implantation. (F) Whole-mount staining of fascia cells labeling VMC. Data are mean \pm s.e.m.; $n = 5$ (7dpi), 8 (14dpi) and 5 (28dpi).

heal with vasculature and functional tissue rather than inducing a typical FBR. Therefore, we set out to investigate the mechanisms underlying the vascularization of regenerative biomaterials using an AAM transplantation model in mice.

On the basis of our findings in this study, we demonstrated that subcutaneous fascia, along with their embedded blood vessels, migrates and encases the AAM implant surface, promoting vascularization and implant function. Using matrix-tracing technique, we observed that the subcutaneous fascia system physically mobilizes to the implant surface, establishing a vascular matrix complex (VMC) in response to AAM implantation. When an impermeable dual surface ePTFE membrane was placed between the fascia and AAM implants, fascia mobilization was blocked, VMC formation was impeded, and the implants became devascularized and collapsed. In agreement with our observations, Ziegler et al. reported that fascia matrix was angiogenic, and the inclusion of fascia tissue in AAM implants significantly enhanced vascularization compared to AAM alone in a rat model [26]. However, the mechanisms by which subcutaneous fascia migrates to encase AAM

implants remain unclear. Previous studies suggest that the ECM movement occurs during organ morphogenesis and early development [27–30], with fibroblasts pulling individual collagen or fibronectin fibers within a 3D culture environment [31]. In deep skin wounds, fascia-derived fibroblasts collectively migrate towards the wound center, moving fascia matrix into the wounds during healing [32]. Our cell-tracing results indicate that fascia-derived fibroblasts are likely responsible for this fascia mobilization. Collectively, our findings highlight the contribution of fascia mobilization to the vascularization and functional outcomes of AAM implants.

Recruiting invasive neovessels from host vasculature ensure circulation between the host and implants. These neovessels must navigate tissue interfaces characterized by gradients and discontinuities in matrix alignment, anisotropy, and density [33]. Interface matrix density, rather than alignment or anisotropy, dictates neovessels invasion into implants [33,34]. High interface matrix density inhibits neovessel invasion into adjacent tissue space, while matrix anisotropy promotes angiogenesis and vascular cell proliferation in a density-dependent manner [35,36].

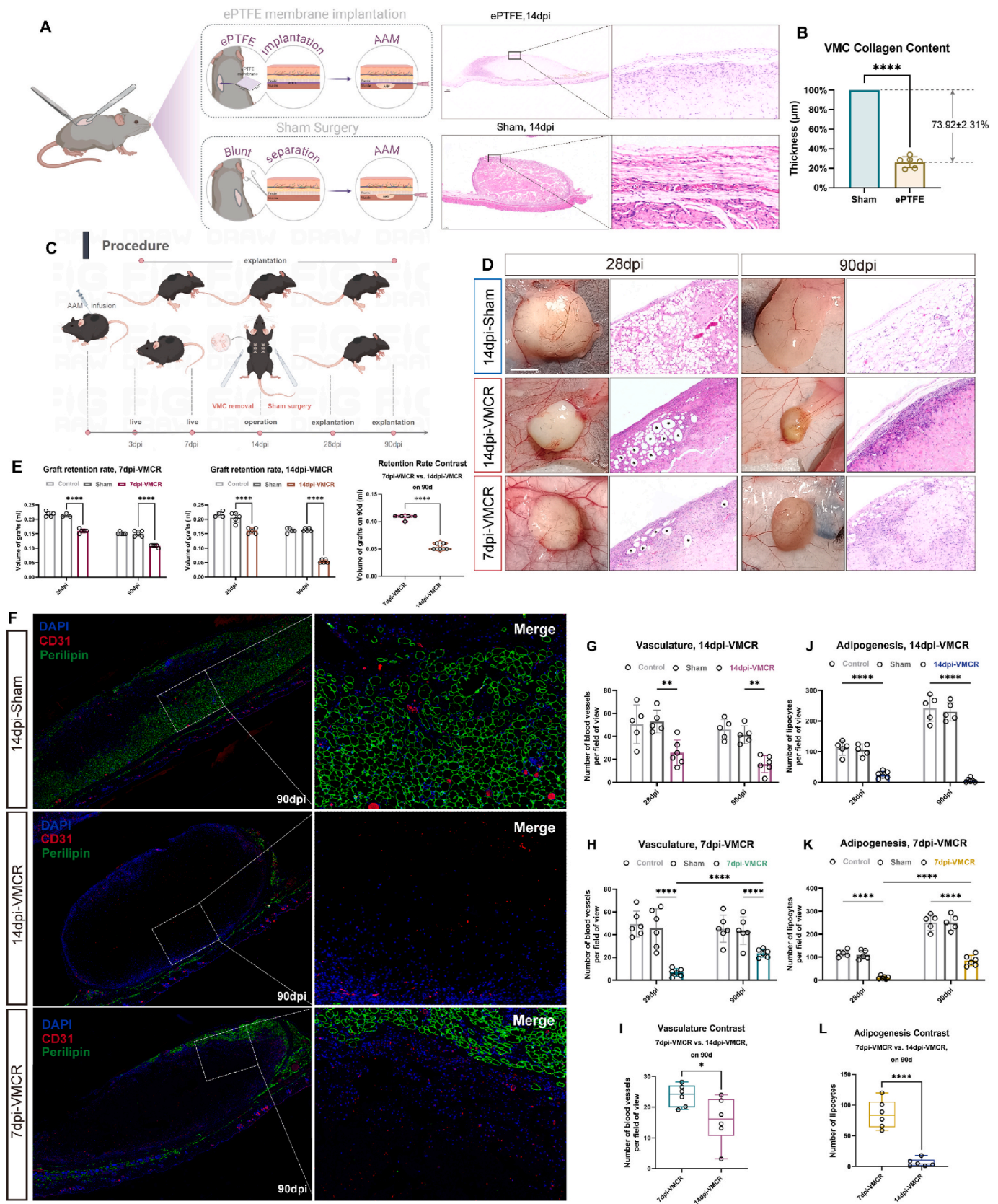


Fig. 5. VMC removal has irreversible impact to AAM angiogenesis and adipogenesis. (A) 16 mm × 8 mm ePTFE membranes were implanted between the subcutaneous fascia and back muscles on the left to block fascia migration (top) and the sham surgery was performed on the right back (bottom). VMC was removed after AAM implantation at 14dpi. (B) Declining VMC collagen content quantified by thickness after ePTFE membrane implantation. Data are mean ± s.e.m.; *t*-test, *n* = 6. 95 % CI. (C) VMC was removed after AAM implantation at 14dpi. (D and E) Morphological images, H&E staining and retention rate of grafts at 28dpi and 90dpi after VMC removal at 7dpi or 14dpi. Black stars indicate the necrotic cavities in the AAM. Two-way ANOVA, *n* = 3 to 5 per group (left and middle); *t*-test, *n* = 5 per group (right). 95 % CI. (F–L) CD31 and perilipin staining and vascularization and adipogenesis impairment of AAM in VMCR model. *N* = 5 to 6 per group. 95 % CI.

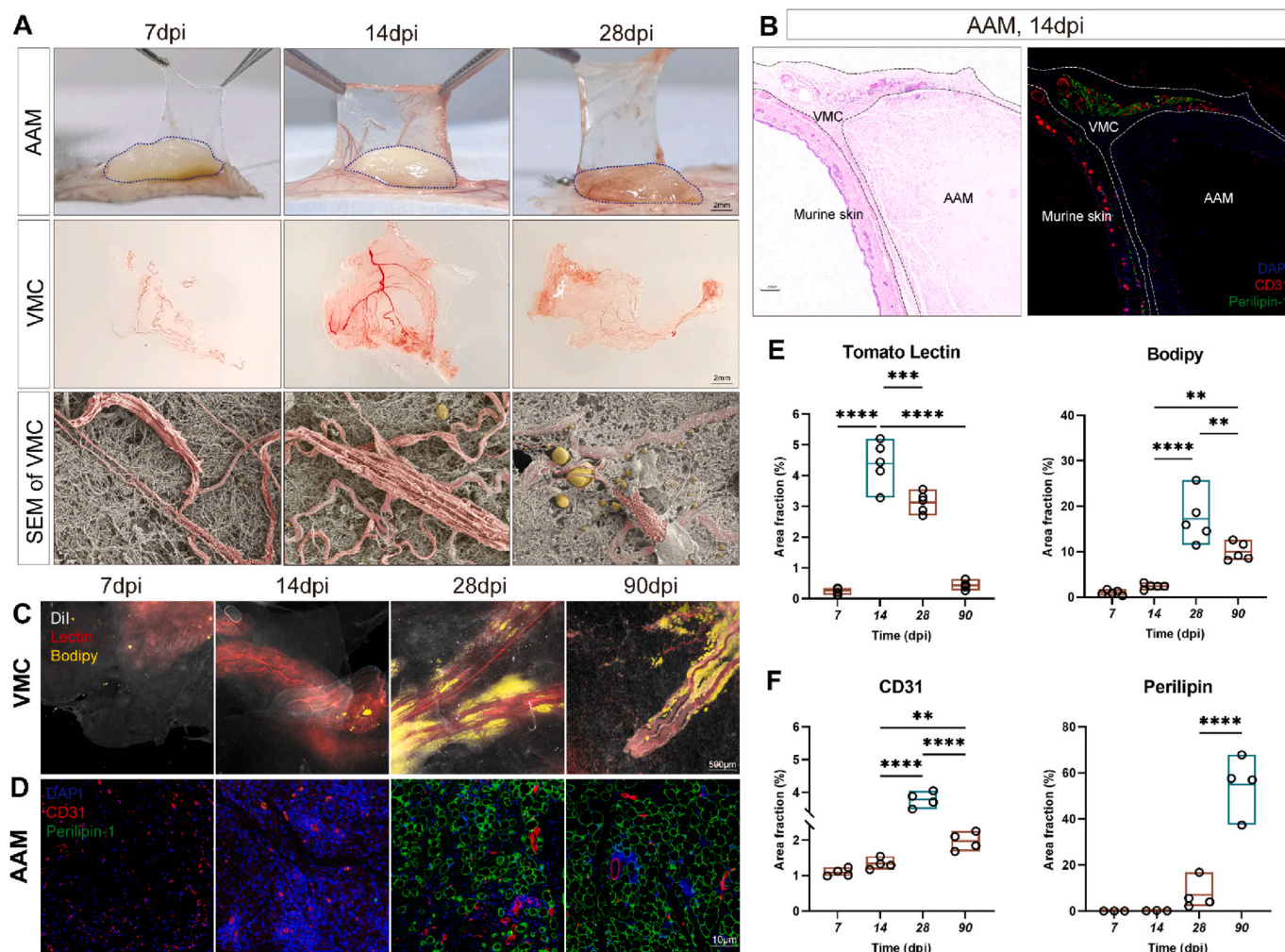


Fig. 6. Pre-vascularization and spontaneous adipogenesis occurred in the early VMC. (A) Morphological images (top and middle) and SEM images (bottom) at 7dpi, 14dpi and 28dpi. (B) CD31 and Perilipin-1 staining for blood vessels and adipocytes. Black and white dotted lines mark the borders between fascia, AAM and murine skin. (C and E) Whole-mount staining of VMC for DiI, Tomato lectin and Bodipy. Comparing to “14 dpi” group, *t*-test, *n* = 4 to 5 per group (left). Comparing to “28 dpi” group, *t*-test, *n* = 5 per group (right). 95 % CI. (D and F) Immunofluorescent staining of AAM for CD31 and Perilipin-1. Comparing to “28 dpi” group, *t*-test, *n* = 4 per group (left). Comparing to “90 dpi” group, *t*-test, *n* = 3 to 4 per group (right). 95 % CI.

Our study found that increasing matrix alignment is positively correlated with growing blood vessels before localized pockets of low density created near the interface at the late stage. This could be explained by the finding that, under the same density, neovessels would rather rearrange and grow (including proliferate, sprout and branch) along the fibril direction than in a vertical direction [37]. Therefore, the increasing alignment localizes the blood vessel development in VMC from the early to middle stages until AAM fibers remodel to a low density. At the late stage, low matrix density in AAM plants and similar matrix density in both VMC and AAM was observed. This low interface matrix density is positively correlated with a high number of blood vessels, suggesting that relaxed AAM fibers recruit VMC vessels to cross the interface at the late stage.

We also found distinct differences in the matrix characteristics deposited on silicone versus AAM surfaces. A mild inflammatory reaction and matrix deposit were observed in VMC compared to fibrous capsules, indicating that the host response to AAM implantation is more akin to healing rather than a typical adverse FBR elicited by silicone. Matrix labeling revealed that fascia tissue contributed to the majority (over 80 %) of VMC, and VMC removal led to obvious destruction and degeneration of AAM implants. Thus, fascia rather than FBR appears to form VMC, supporting the vascularization and implant function in vivo. Collagen characteristics in VMC undergo consistent changes in vivo in a

process known as matrix remodeling [38,39]. Transplantation of ECM biomaterials leads to tissue damage that triggers inflammatory responses, which, in turn, strongly participates in the matrix remodeling of the ECM biomaterials [40]. Inflammation-mediated matrix remodeling, which requires a myriad of orchestrated interactions between many cell types, enzymes, and cytokines, determines the outcomes of biomaterials implants [41,42]. Early pro-inflammation reactions, characterized by expression of neutrophils and M1 macrophages, may lead to the degradation of the biomaterials and drive the ECM into a fetal-like state. ECM degradation leads to the release of matrix-related bioactive components that leads to pro-regenerative reactions at the transplantation sites. Afterwards, pro-inflammatory cells gradually fade away along with the appearance of, anti-inflammatory reaction, which involves macrophage polarization to the M2 phenotype and leukocyte activation to T helper 2 (Th2) cells. These anti-inflammatory cells interact with each other to facilitate matrix deposition and tissue reconstruction. Fetal-like ECM then switches to a mature state due to matrix deposition, which is beneficial for homeostasis and maturation of regenerative tissue. As key regulators of ECM remodeling, stromal fibroblasts may influence collagen arrangement and density via ECM synthesis and LOX-mediated cross-linking [43,44]. These activities could be regulated by macrophage-derived signals, with M1 macrophages driving ECM degradation and realignment, and M2 macrophages facilitating

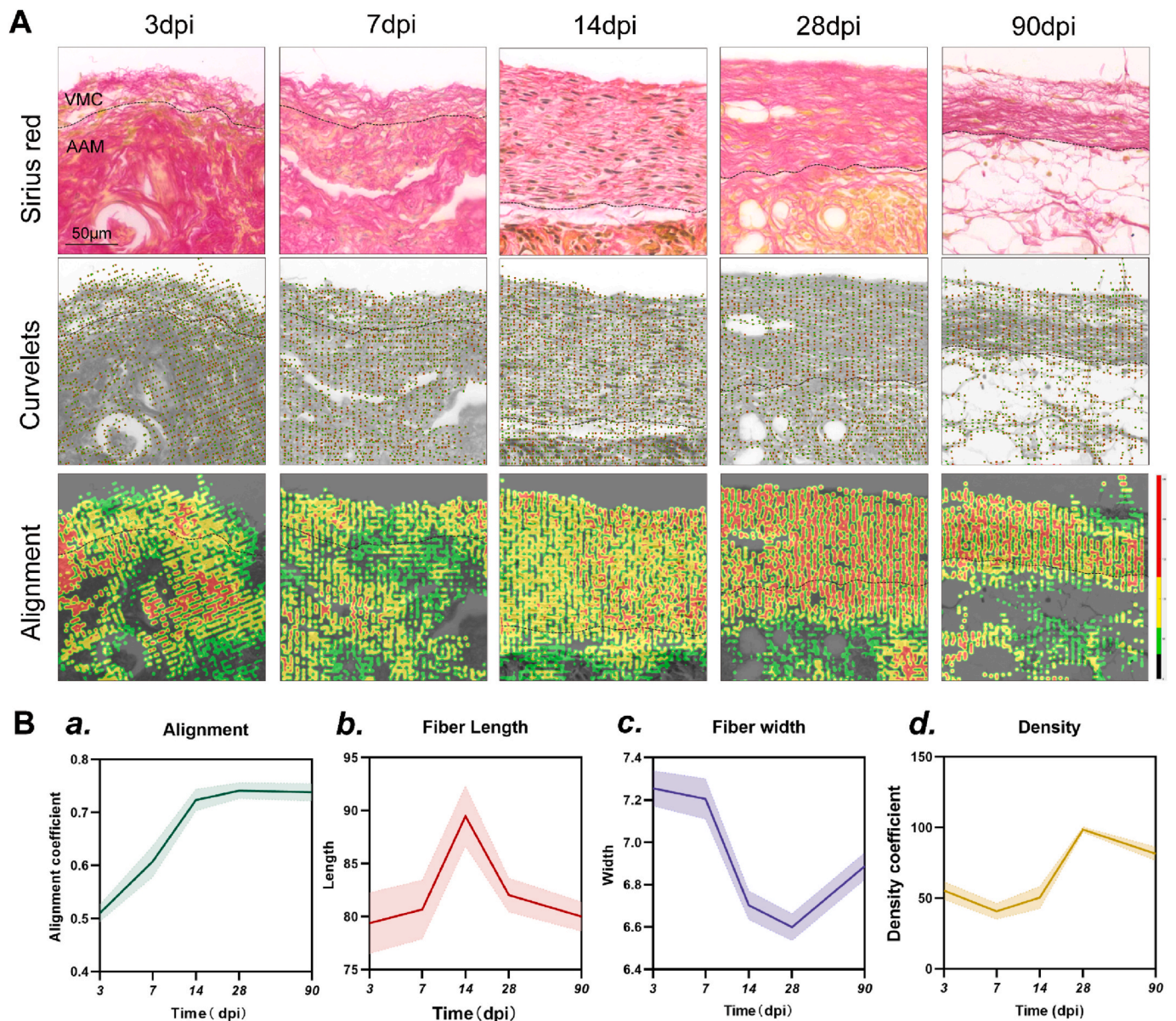


Fig. 7. Dynamic changes of fiber characteristics of fascia-derived VMC. (A) Sirius red staining of grafts and Curvelet transformation, alignment heatmap and single fiber extraction based on the images, to analyze the architectural of VMC fiber. Black dotted lines separate the VMC from AAM. Red dots indicate the center of fiber segments; green lines indicate the fiber orientation in Curvelets transformation. (B) Alignment, length, width and density of VMC fiber change over time.

Col-III and Col-IV deposition, supporting matrix stabilization[45–47]. In this study, our findings revealed a progressive increase in the collagen III/I ratio in VMC from 3 to 14 dpi, followed by a decline. This trend parallels vascular development within VMC, suggesting a remodeling process that mimics fetal ECM. Fetal ECM, known for its high repair and regenerative potential, exhibits a greater collagen III/I ratio compared to mature ECM, supporting its association with vasculature formation at 14 dpi [48,49]. These observations indicate that VMC transitions to a fetal-like ECM state to facilitate vascularization. However, the precise inflammatory mechanisms and cellular interactions driving VMC matrix remodeling warrant further investigation.

Spontaneous adipogenesis was found in VMC in this study, indicating that adipocytes can originate from non-adipose tissue. Previous studies have identified that outgrown cells from superficial fascia tissue express a significant amount of adipose progenitor cells (APCs) markers, including CD44, CD90, CD29, α -SMA, PDGFR β and CD106. These fascia-derived cells were able to differentiate into adipocytes [50,51], which may partly explain the spontaneous adipogenesis observed in the surface

matrix of this study. Notably, adipogenesis were mainly located along vessels in VMC. It has been generally accepted that APCs are a subset of perivascular mural cells that adhere to vessels and differentiate into adipocytes upon adipogenic cues. It is therefore we suggest that APC in fascia vasculature underwent adipogenesis during the remodeling process of VMC. Overall, our data provide more evidence for the fascial origin of adipocytes, which may strengthen the understanding of metabolic regulation between fascia-derived adipose tissue and other organs, providing new insight into the treatment of metabolic diseases or obesity.

This study provide novel insights into the vascularization process of regenerative biomaterials, and several aspects still deserve attention. First, although the histology of fascia tissue is relatively simple, their intrinsic features, such as matrix substance, cell composition, and cell functions, vary largely depending on anatomic locations and species [16,37]. Thus, the mobility and beneficial role of fascia tissue deserve more investigation in different species and anatomic sites. Second, the molecular mechanisms and cell populations that orchestrate the

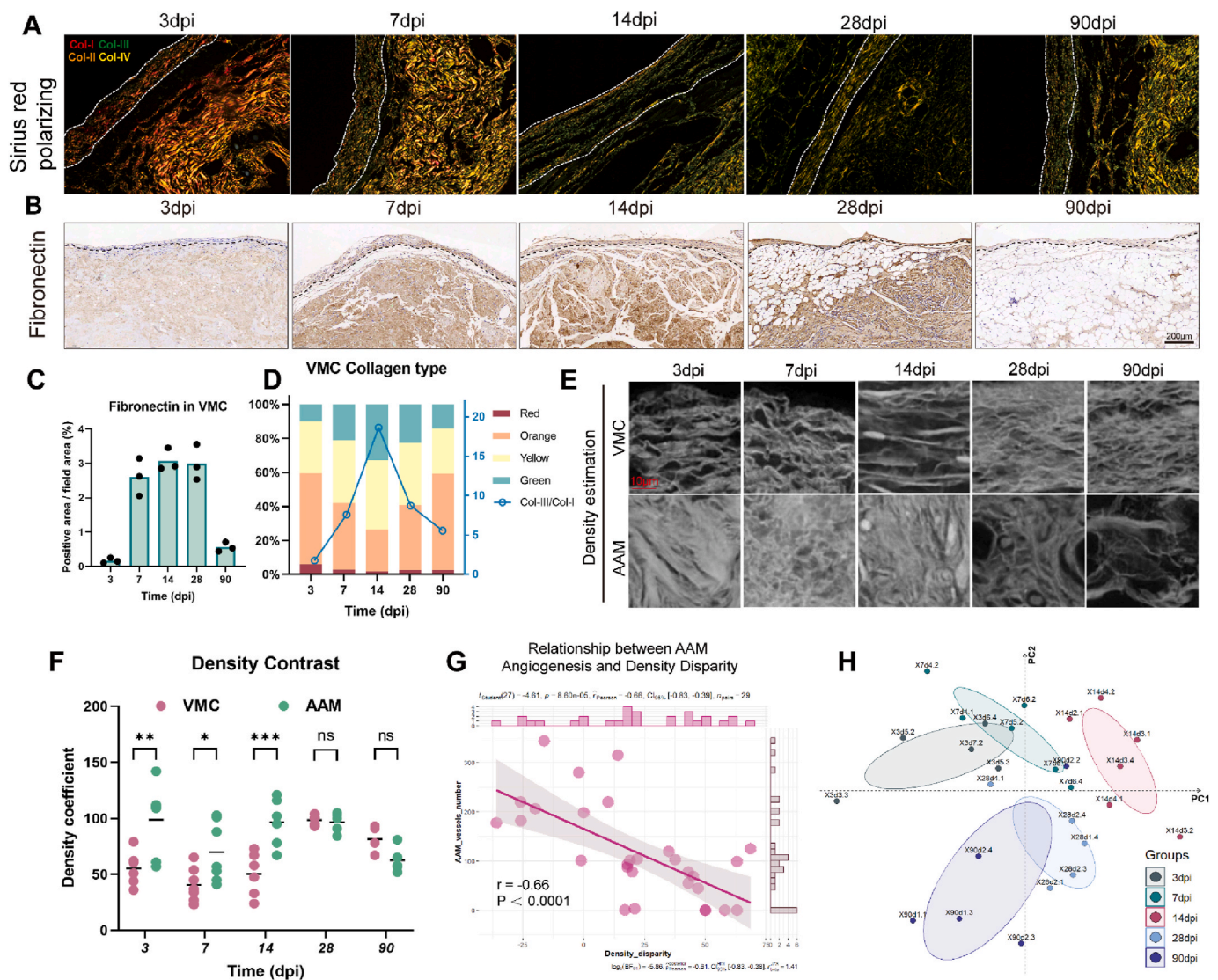


Fig. 8. Dynamic changes of fiber types of VMC and density disparity between VMC and AAM. (A and D) Sirius red polarizing images for collagen type identification of VMC. White dotted lines indicate the range of VMC. (B and C) Fibronectin staining for basement membrane proteins in VMC. $N = 3$ per group. 95 % CI. (E and F) Density of VMC and AAM and density disparity between VMC and AAM on histologic images by CT-Fire. Pairwise comparisons between VMC and AAM, t -test, $n = 6$ per group. 95 % CI. (G) Correlation analysis of AAM blood vessels number and density disparity between VMC and AAM. Spearman's correlation analysis, $n = 29$ pairs. 95 % CI. (H) PCA on output parameters of fiber characteristics, including collagen type and fiber architecture of VMC.

mobility of subcutaneous fascia system to encase implanted biomaterials require investigation in ongoing studies using single-cell sequencing and genetic lineage method. Third, ECM remodeling process was found during the migration of subcutaneous fascia, it is therefore reasonable to investigate the remodeling in VMC. Notably, spontaneous adipogenesis was observed specifically in VMC rather than normal fascia, suggesting a pro-adipogenic microenvironment within the VMC. Further study of the adiogenic microenvironment in VMC would benefit our understanding of adipose tissue engineering. The study of fasciology is relatively understudied, especially in the field of regenerative biomaterials. At present, biomaterials research mainly focus on the design of the materials themselves or addition of pro-vascular factors. This study demonstrated the importance of subcutaneous fascia in the vascularization of implanted biomaterials; thus, targeted regulation of fascia tissue would be a new direction in improving the success of biomaterials applications in regenerative medicine. Given its accessibility and prevalence, subcutaneous fascia tissue also holds potential as a pro-angiogenic and progenitor source for tissue engineering applications, such as soft tissue repair and wound healing.

5. Conclusions

In this study, we show that the mobilization of subcutaneous fascia helps form new blood vessels in AAM implants by drawing in surrounding blood vessels to create a supportive vascular matrix on the implant surface. This supportive matrix exhibited active changes in its structure, which may further facilitate the implants vascular connection with the surrounding tissue in vivo. Our findings emphasize the crucial role of subcutaneous fascia in vascularization and adipogenesis of AAM implants, offering novel knowledge and targeted regulation for guaranteeing long-term survival and function of regenerative biomaterials.

CCRediT authorship contribution statement

Han Yang: Writing – review & editing, Writing – original draft, Visualization, Methodology, Formal analysis, Data curation. **Yidan Xu:** Methodology, Formal analysis. **Sousan Cheong:** Writing – original draft. **Cuiying Xie:** Visualization, Methodology, Formal analysis, Data curation. **Yufan Zhu:** Visualization, Methodology. **Shujie Xu:**

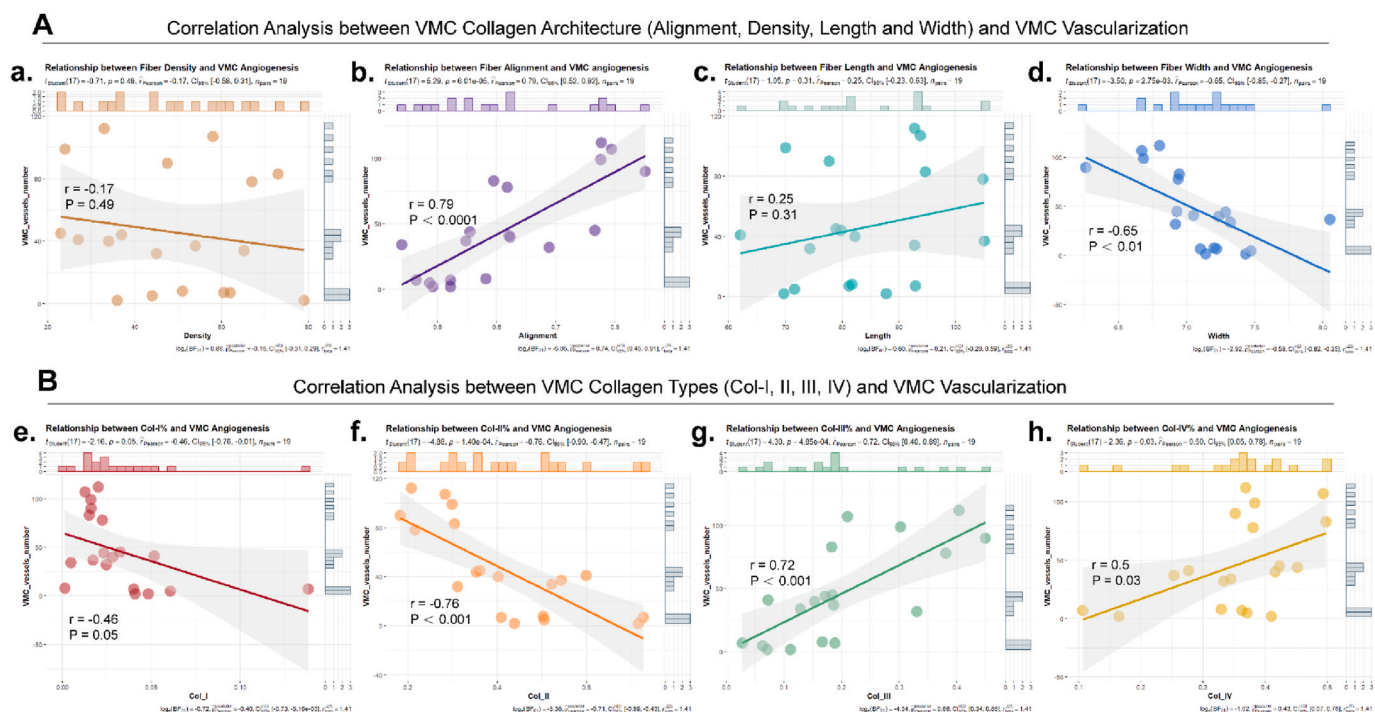


Fig. 9. Collagen remodeling and vasculature development in VMC and AAM at the early and middle stage. (A) Correlation analysis of VMC blood vessels number and VMC collagen fiber architecture. Spearman’s correlation analysis, n = 19 pairs. 95 % CI. (B) Correlation analysis of VMC blood vessels number and VMC collagen fiber types. Spearman’s correlation analysis, n = 19 pairs. 95 % CI.

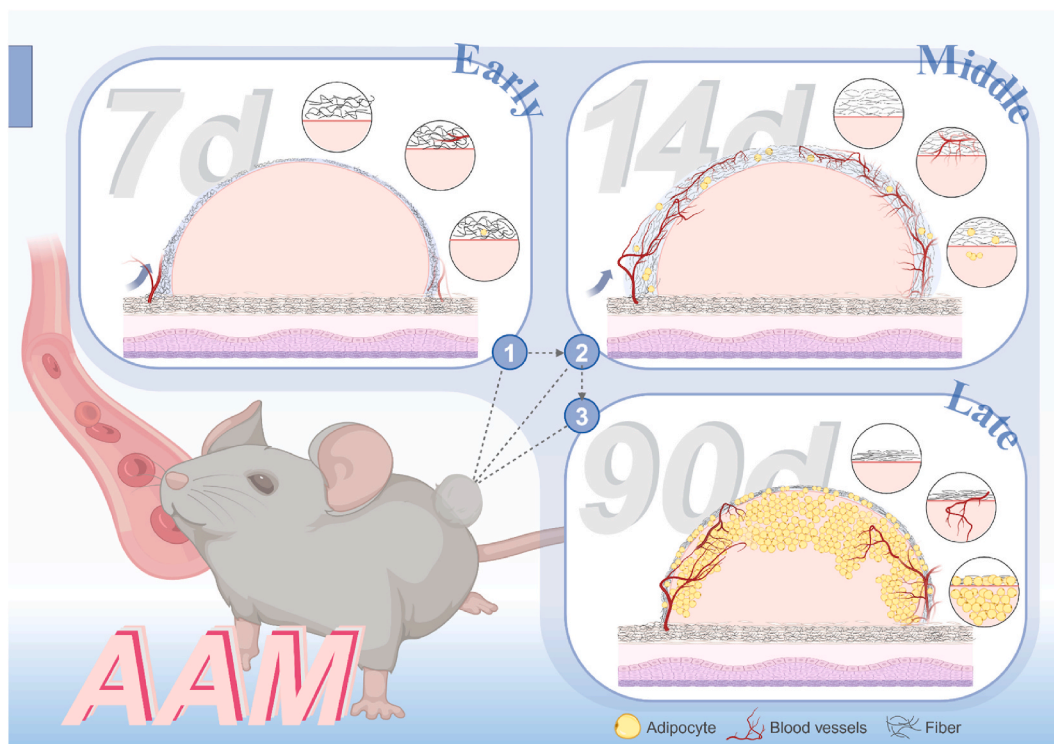


Fig. 10. Subcutaneous fascia-mediated vascularization and function of AAM. Mobilization of subcutaneous fascia contributed to the vascularization of AAM implants by dragging their surrounding fascia-embedded blood vessels to form a VMC on the implant surface at early and middle stage. VMC exhibited a dynamic matrix remodeling process and facilitated the AAM implants vascularization and function at late stage. Created with Biorender (<https://biorender.com/>).

Methodology, Data curation. **Feng Lu:** Funding acquisition, Conceptualization. **Yunfan He:** Writing – review & editing, Writing – original draft, Conceptualization.

Funding

This work was supported by National Natural Science Foundation of

China (Grant No. 82072196, 82102350, 82002058 and 82372544), Guangdong Basic and Applied Basic Research Foundation (Grant No. 2023A1515011741), Guangzhou Science and Technology Program Key Project (Grant No. 2023A04J2353), and Guangdong Medical Science and Technology Research Fund (Grant No. B2022267).

Declaration of competing interest

The authors declared no potential conflict of interest with respect to the research, authorship, and/or publication of this article. The research was conducted in the absence of any commercial or financial relationships that could be construed as a potential conflict of interest.

Data availability

No data was used for the research described in the article.

References

- M.N. Rahaman, J.J. Mao, Stem cell-based composite tissue constructs for regenerative medicine, *Biotechnol. Bioeng.* 91 (2005) 261–284.
- J. Rouwkema, B.F.J.M. Koopman, C.A.V. Blitterswijk, et al., Supply of nutrients to cells in engineered tissues, *Biotechnol. Genet. Eng. Rev.* 26 (2009) 163–178.
- E.C. Novosel, C. Kleinhaus, P.J. Kluger, Vascularization is the key challenge in tissue engineering, *Adv. Drug Deliv. Rev.* 63 (2011) 300–311.
- W.Y. Wang, R.N. Kent, S.A. Huang, et al., Direct comparison of angiogenesis in natural and synthetic biomaterials reveals that matrix porosity regulates endothelial cell invasion speed and sprout diameter, *Acta Biomater.* 135 (2021) 260–273.
- M.R. Major, V.W. Wong, E.R. Nelson, et al., The foreign body response: at the interface of surgery and bioengineering, *Plast. Reconstr. Surg.* 135 (2015) 1489–1498.
- J.D. Bryers, C.M. Giachelli, B.D. Ratner, Engineering biomaterials to integrate and heal: the biocompatibility paradigm shifts, *Biotechnol. Bioeng.* 109 (2012) 1898–1911.
- F. Boccafroschi, C. Mosca, M. Cannas, Cardiovascular biomaterials: when the inflammatory response helps to efficiently restore tissue functionality?: inflammatory response to cardiovascular biomaterials, *J. Tissue Eng. Regen. Med.* 8 (2014) 253–267.
- J.M. Anderson, A. Rodriguez, D.T. Chang, Foreign body reaction to biomaterials, *Semin. Immunol.* 20 (2008) 86–100.
- B.N. Brown, S.F. Badylak, Expanded applications, shifting paradigms and an improved understanding of host–biomaterial interactions, *Acta Biomater.* 9 (2013) 4948–4955.
- A.H. Morris, D.K. Stamer, T.R. Kyriakides, The host response to naturally-derived extracellular matrix biomaterials, *Semin. Immunol.* 29 (2017) 72–91.
- K. Liu, Y. He, Y. Yao, et al., Methoxy polyethylene glycol modification promotes adipogenesis by inducing the production of regulatory T cells in xenogeneic acellular adipose matrix, *Mater. Today Bio.* 12 (2021) 100161.
- M. Lin, J. Ge, X. Wang, et al., Biochemical and biomechanical comparisons of decellularized scaffolds derived from porcine subcutaneous and visceral adipose tissue, *J. Tissue Eng.* 10 (2019), 2041731419888168.
- Y. He, M. Lin, X. Wang, et al., Optimized adipose tissue engineering strategy based on a neo-mechanical processing method, *Wound Repair Regen.* 26 (2018) 163–171.
- X. Bi, B. Li, J. Zou, et al., Fascia promotes adipose tissue regeneration by improving early macrophage infiltration after fat grafting in a mouse model, *Plast. Reconstr. Surg.* 152 (2023) 446e–457e.
- C. Stecco, V. Macchi, A. Porzionato, et al., The fascia: the forgotten structure, *Ital. J. Anat. Embryol. Arch. Ital. Anat. Ed. Embriol.* 116 (2011) 127–138.
- M.F. Abu-Hijleh, A.L. Roshier, Q. Al-Shboul, et al., The membranous layer of superficial fascia: evidence for its widespread distribution in the body, *Surg. Radiol. Anat.* 28 (2006) 606–619.
- M. Xu, Y. He, Y. Li, et al., Combined use of autologous sustained-release scaffold of adipokines and acellular adipose matrix to construct highly vascularized, mature, engineered adipose tissue, *Plast. Reconstr. Surg.* 153 (2) (2024) 348e–360e.
- D. Correa-Gallegos, D. Jiang, S. Christ, et al., Patch repair of deep wounds by mobilized fascia, *Nature* 576 (2019) 287–292.
- A.I. Cassidy, N.M. Hidir, L. Grøndahl, Enhancing expanded poly (tetrafluoroethylene) (ePTFE) for biomaterials applications, *J. Appl. Polym. Sci.* 131 (app) (2014) 40533.
- Y. Roina, F. Auber, D. Hocquet, et al., ePTFE -based biomedical devices: an overview of surgical efficiency, *J. Biomed. Mater. Res. B Appl. Biomater.* 110 (2022) 302–320.
- Y. Liu, A. Keikhosravi, G.S. Mehta, et al., Methods for quantifying fibrillar collagen alignment, *Methods Mol. Biol. Clifton NJ* 1627 (2017) 429–451.
- D. Zhang, W. Zhao, Q. Fang, et al., The efficacy of fractional CO₂ laser in acne scar treatment: a meta-analysis, *Dermatol. Ther.* 34 (2021).
- Y. Wen, H. Yang, J. Wu, et al., COL4A2 in the tissue-specific extracellular matrix plays important role on osteogenic differentiation of periodontal ligament stem cells, *Theranostics* 9 (2019) 4265–4286.
- E. Dondossola, B.M. Holzapfel, S. Alexander, et al., Examination of the foreign body response to biomaterials by nonlinear intravital microscopy, *Nat. Biomed. Eng.* 1 (2016) 7.
- Z. Sheikh, P.J. Brooks, O. Barzilay, et al., Macrophages, foreign body giant cells and their response to implantable biomaterials, *Materials* 8 (2015) 5671–5701.
- M.E. Ziegler, A.M. Sorensen, D.A. Banyard, et al., Deconstructing allograft adipose and fascia matrix: fascia matrix improves angiogenesis, volume retention, and adipogenesis in a rodent model, *Plast. Reconstr. Surg.* 151 (2023) 108–117.
- E.A. Zamir, B.J. Rongish, C.D. Little, The ECM moves during primitive streak formation—computation of ECM versus cellular motion, *PLoS Biol.* 6 (2008) e247.
- A. Szabó, P.A. Rupp, B.J. Rongish, et al., Extracellular matrix fluctuations during early embryogenesis, *Phys. Biol.* 8 (2011) 045006.
- A. Aleksandrova, A. Czirók, A. Szabó, et al., Convective tissue movements play a major role in avian endocardial morphogenesis, *Dev. Biol.* 363 (2012) 348–361.
- R. Loganathan, B.J. Rongish, C.M. Smith, et al., Extracellular matrix motion and early morphogenesis, *Dev. Camb. Engl.* 143 (2016) 2056–2065.
- M. Miron-Mendoza, V. Koppaka, C. Zhou, et al., Techniques for assessing 3-D cell-matrix mechanical interactions in vitro and in vivo, *Exp. Cell Res.* 319 (2013) 2470–2480.
- L. Wan, D. Jiang, D. Correa-Gallegos, et al., Connexin43 gap junction drives fascia mobilization and repair of deep skin wounds, *Matrix Biol.* 97 (2021) 58–71.
- S.A. LaBelle, S.S. Dinkins, J.B. Hoying, et al., Matrix anisotropy promotes angiogenesis in a density-dependent manner, *Am. J. Physiol. Heart Circ. Physiol.* 322 (2022) H806–H818.
- S.A. LaBelle, A.M. Poulson, S.A. Maas, et al., Spatial configurations of 3D extracellular matrix collagen density and anisotropy simultaneously guide angiogenesis, *PLoS Comput. Biol.* 19 (2023) e1011553.
- H.A. Strobel, J.B. Hoying, The evaluation of neovessel angiogenesis behavior at tissue interfaces, *Methods Mol. Biol. Clifton NJ* 2441 (2022) 311–320.
- H.A. Strobel, S.A. LaBelle, L. Krishnan, et al., Stromal cells promote neovascular invasion across tissue interfaces, *Front. Physiol.* 11 (2020) 1026.
- X. Su, Y. Lyu, W. Wang, et al., Fascia origin of adipose cells, *Stem Cell.* 34 (2016) 1407–1419.
- A.E. Fetz, M.Z. Radic, G.L. Bowlin, Neutrophils in biomaterial-guided tissue regeneration: matrix reprogramming for angiogenesis, *Tissue Eng., Part B* 27 (2021) 95–106.
- M. Xu, T. Su, X. Jin, et al., Inflammation-mediated matrix remodeling of extracellular matrix-mimicking biomaterials in tissue engineering and regenerative medicine, *Acta Biomater.* 151 (2022) 106–117.
- A.V. Piterina, A.J. Cloonan, C.L. Meaney, et al., ECM-based materials in cardiovascular applications: inherent healing potential and augmentation of native regenerative processes, *Int. J. Mol. Sci.* 10 (2009) 4375–4417.
- J.M. Aamodt, D.W. Grainger, Extracellular matrix-based biomaterial scaffolds and the host response, *Biomaterials* 86 (2016) 68–82.
- C. Bonnans, J. Chou, Z. Werb, Remodelling the extracellular matrix in development and disease, *Nat. Rev. Mol. Cell Biol.* 15 (2014) 786–801.
- K. Pfisterer, L.E. Shaw, D. Symmank, et al., The extracellular matrix in skin inflammation and infection, *Front. Cell Dev. Biol.* 9 (2021).
- M. D'Urso, N.A. Kurniawan, Mechanical and physical regulation of fibroblast–myofibroblast transition: from cellular mechanoreponse to tissue pathology, *Front. Bioeng. Biotechnol.* 8 (2020).
- S. Psarras, The macrophage–fibroblast dipole in the context of cardiac repair and fibrosis, *Biomolecules* 14 (2024) 1403.
- C. Zhao, Z. Yang, Y. Li, et al., Macrophages in tissue repair and regeneration: insights from zebrafish, *Cell Regen.* 13 (2024) 12.
- M. Gou, H. Wang, H. Xie, et al., Macrophages in guided bone regeneration: potential roles and future directions, *Front. Immunol.* 15 (2024) 1396759.
- J.R. Merkel, B.R. DiPaolo, G.G. Hallock, et al., Type I and type III collagen content of healing wounds in fetal and adult rats, *Proc. Soc. Exp. Biol. Med. Soc. Exp. Biol. Med. N Y N* 187 (1988) 493–497.
- G.G. Hallock, D.C. Rice, J.R. Merkel, et al., Analysis of collagen content in the fetal wound, *Ann. Plast. Surg.* 21 (1988) 310–315.
- W.P. Cawthorn, E.L. Scheller, O.A. MacDougald, Adipose tissue stem cells meet preadipocyte commitment: going back to the future, *J. Lipid Res.* 53 (2012) 227–246.
- M.-Y. Choi, H.-I. Kim, Y.-I. Yang, et al., The isolation and in situ identification of MSCs residing in loose connective tissues using a niche-preserving organ culture system, *Biomaterials* 33 (2012) 4469–4479.